

1 Anomalous Hall effect in electrolytically 2 reduced PdCoO₂ thin films

3

4 Yiting Liu,^{a,b,†} Gaurab Rimal,^{b,†} Pratyankara Narasimhan,^b Seongshik Oh^{b,*}

5

6 ^a State Key Laboratory of Precision Spectroscopy, East China Normal University,
7 Shanghai 200062, China

8 ^b Department of Physics & Astronomy, Rutgers, The State University of New Jersey,
9 Piscataway, New Jersey 08854, USA

10 [†]These authors contributed equally to this work.

11 ^{*} Corresponding author: ohsean@physics.rutgers.edu

12

13 Abstract

14 PdCoO₂, being highly conductive and anisotropic, is a promising material for fundamental
15 and technological applications. Recently, reduced PdCoO₂ thin films were shown to exhibit
16 ferromagnetism after hydrogen annealing. Here, we demonstrate that when PdCoO₂ film is
17 used as a cathode for dissociation of water, hydrogen generated around the film reduces the
18 material and leads to the emergence of anomalous Hall effect (AHE). Moreover, we
19 demonstrate that the sign of the AHE signal can also be changed with the electrolytic process.
20 Electrolytically-modified PdCoO₂ films may open a door to applications in spintronics.

21

22 Keywords: Thin films; Delafossite; Palladium Cobalt Oxide; Hydrogenation; Anomalous
23 Hall effect; Electrolysis

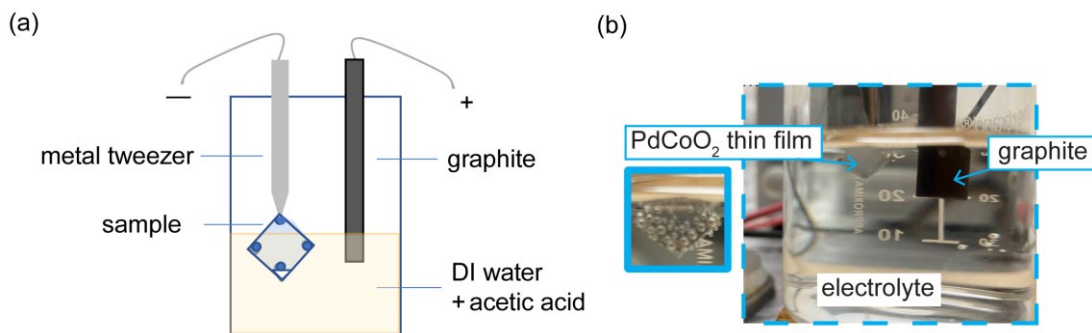
24

25 1. Introduction

26 PdCoO₂ is a promising oxide with a unique quasi-two-dimensional electronic structure.
27 It has alternating Pd and CoO₂ layers, with each layer having a triangular lattice. Contributed
28 mainly by Pd layers, PdCoO₂ has room-temperature conductivity comparable to those of the
29 most conductive metals, such as copper, silver and gold [1]. Although PdCoO₂ and other
30 delafossites were first synthesized in 1971 [2,3], PdCoO₂ was largely ignored for decades.
31 However, following the synthesis of high quality single crystals in recent years [4–6], there
32 has been renewed interest in this system for the study of properties such as the thermoelectric
33 power [7–9], electronic structure [10–12] and high anisotropy in structure, conductivity and
34 compression behavior [13–15]. First-principles calculations suggest that the high in-plane
35 conductivity of PdCoO₂ originates mostly from the Pd band [10]. Hicks *et al.* also presented
36 high-resolution de Haas-van Alphen oscillations and obtained a long mean free path of
37 ~20 μm at 10 K [16], which is the longest among any oxide. Subsequently, hydrodynamic
38 transport was observed in this material, which allowed the determination of electronic
39 viscosity [17].

40 Delafossites were also studied as part of electrodes and catalysts in water electrolysis
41 [18–20]. Hinogami *et al.* investigated catalytic activities of copper delafossites, such as
42 CuFeO₂ and CuCoO₂ [21,22]. Podjaski *et al.* found that Co dissolution in the electrolyte and
43 Pd-rich surface layer in PdCoO₂ promotes electrolysis efficiency [18]. Li *et al.* demonstrated
44 that upon electrolysis of PdCoO₂ bulk crystals, Pd nanoclusters and Co oxides form and lead
45 to high-efficiency hydrogen evolution [19].

46 PdCoO₂ is only weakly paramagnetic, but shows signatures of surface magnetism on
 47 Pd terminated surfaces [23]. Harada *et al.* found thickness-dependent anomalous Hall effect
 48 in PdCoO₂ thin films [24], and more recently, Rimal *et al.* demonstrated that reduction of
 49 PdCoO₂ thin films via hydrogen annealing can exhibit strong ferromagnetism with
 50 perpendicular magnetic anisotropy (PMA) [25], which was mainly as a result of oxygen loss
 51 and subsequent transformation of PdCoO₂ film into an atomically-intermixed Pd-Co alloy.
 52 Here, we show that the electronic properties of PdCoO₂ films can be substantially modified
 53 via electrolysis. By using different cathode voltages for water splitting (i.e. hydrogen
 54 generation) and studying the evolution of Hall effect, we find that PdCoO₂ films are reduced,
 55 exhibit ferromagnetism, and show different signs of anomalous Hall effect (AHE) depending
 56 on the applied voltage.



57
 58 **Figure 1:** Experiment setup. (a) Schematic diagram of the setup; (b) Underwater part of the
 59 film. Also shown is the formation of hydrogen bubbles on the film surface when a voltage of
 60 -5.0 V is applied.

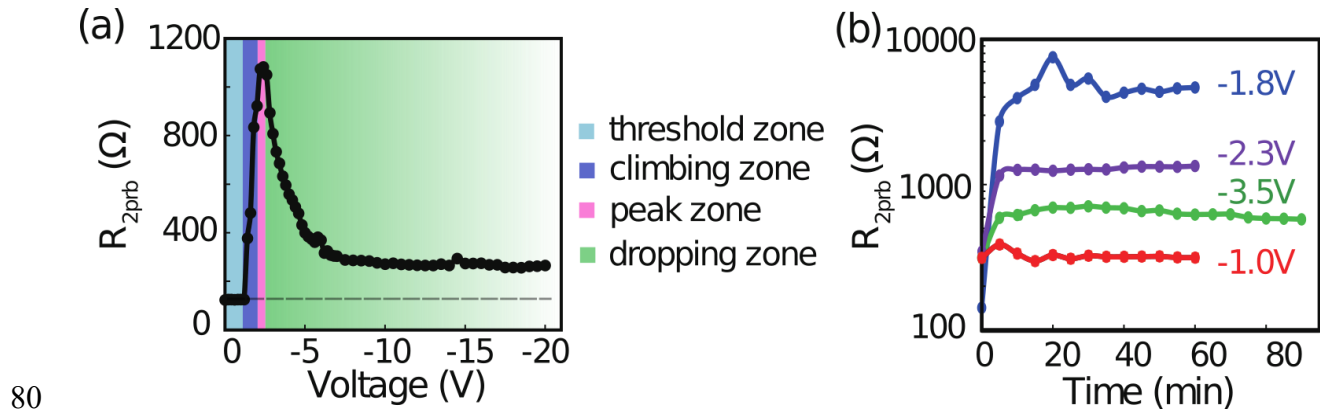
61

62 2. Experimental details

63 For this study, we utilized 9 nm thick PdCoO₂ thin films, grown on 10 × 10 mm², Al₂O₃
 64 (0001) substrate using oxygen plasma-assisted molecular beam epitaxy with a base pressure
 65 of low 10⁻⁸ Pa [26]. After growth, the sample is cut into four pieces which are used for four

66 separate experiments. Before each electrolysis experiment, indium dots are bonded to the
 67 sample corners as contact points for electrical measurements as shown in Figure 1(a,b). A
 68 metal tweezer holds the film just above the water level, while a graphite rod is used as the
 69 second electrode. Unless stated otherwise, PdCoO_2 is used as the negative electrode. We used
 70 30 mL water with 2 drops of acetic acid as the electrolyte to facilitate hydrogen evolution.
 71 Electrolysis is powered by a variable voltage source. After each process, we measured the
 72 average two-probe resistance between indium contacts ($R_{2\text{prb}}$) on the corners of the film using
 73 a multimeter. Afterwards, Hall effect measurements were carried out using van der Pauw
 74 method. XPS was done on as-prepared samples using ThermoFisher K-alpha system using
 75 monochromated Al K- α beam (1486.7 eV). The XPS binding energy and resolution was
 76 calibrated using Ag 3d_{5/2} line on a clean Ag surface. Rutherford backscattering spectrometry
 77 (RBS) was performed at Rutgers ion scattering facility using 2 MeV He^{2+} ions.
 78

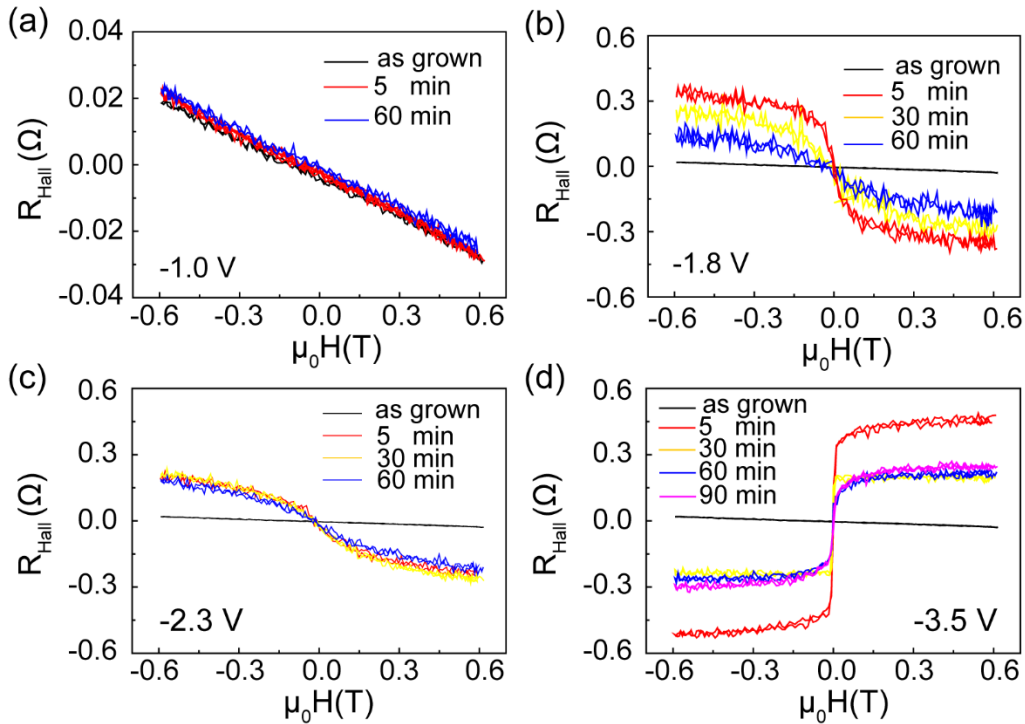
79 3. Results and discussion



80
 81 **Figure 2:** Average two-point resistance ($R_{2\text{prb}}$) measured after a sample is kept in the
 82 electrolyte (a) at the specified voltage for 5 minutes and (b) for the specified time at -1.0 V, -
 83 1.8 V, -2.3 V and -3.5 V. Four separate samples are used for (b). The negative voltages imply
 84 that the PdCoO_2 film is used as a cathode.

85 In Figure 2(a), we show how the applied voltage affects the film. Below -1.2 V, the
86 film resistance remains unchanged, because no hydrogen is generated: note that this voltage
87 is consistent with the well-known water splitting potential of -1.23 V. This region is termed
88 the *threshold zone*. A steep increase occurs just above this threshold voltage and the
89 resistance peaks at about -2.4 ± 0.2 V and slightly plateaus to about -2.6 V. The voltage
90 range of -1.2 V to -2.2 V is thus termed the *climbing zone* and -2.2 V to -2.6 V is the *peak*
91 *zone*. Past the peak zone, in the region termed *dropping zone*, the resistance starts to decrease
92 gradually and reaches a stable value after -7.5 V. The resistance for the stable zone is higher
93 than that of the original film. When we used PdCoO_2 film as an anode, the film remained
94 unaffected up to the maximum applied voltage of 5.0 V.

95 In Figure 2(b), we present how the film resistance changes as a function of the process
96 time for each of the four zones: *threshold* (-1.0 V), *climbing* (-1.8 V), *peak* (-2.3 V) and
97 *dropping zone* (-3.5 V), respectively. While in the threshold zone (-1.0 V), the film resistance
98 remains stable around the initial value, suggesting no changes in the film. This is because no
99 hydrogen is evolved, so the film remains unaffected. For all the other zones the resistance
100 rises fast initially and stabilizes after about 20 minutes. Interestingly, the stabilized resistance
101 is highest at -1.8 V and decreases at higher voltages. This trend is similar to our earlier work
102 on hydrogenation of PdCoO_2 films, in which the resistance initially rises with gradual oxygen
103 removal and then drops after extended annealing [25].

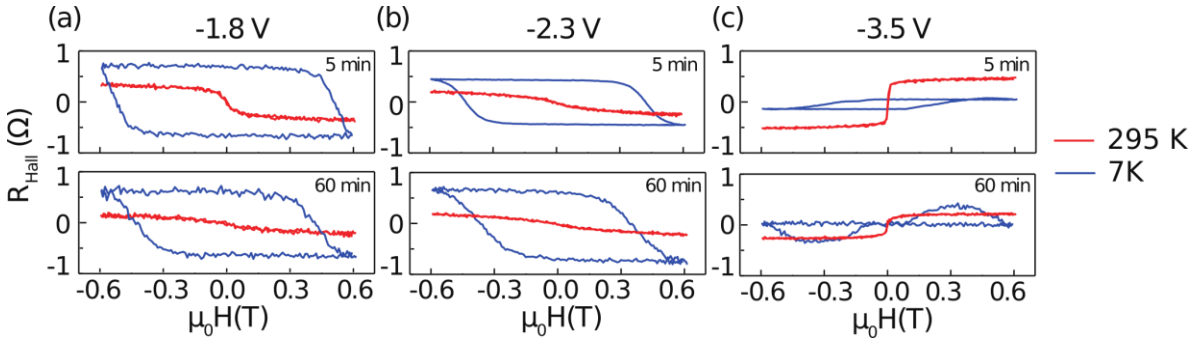


104

105 **Figure 3:** Hall effect data ($R_{Hall} \equiv R_{xy}$) of $PdCoO_2$ thin films measured at room temperature
 106 after electrolytic processing at (a) -1.0 V, (b) -1.8 V, (c) -2.3 V and (d) -3.5 V.

107 To determine the nature of the resulting films, we investigated their transport behavior.
 108 The room temperature Hall effect is shown in Figure 3. The as-grown $PdCoO_2$ film shows
 109 clear n-type linear behavior, and no change is observed for applied voltage of -1.0 V. Past
 110 this threshold voltage, AHE is present, as shown in Figure 3(b-d). It is notable that at the
 111 highest voltage (-3.5 V, Figure 3(d)), the AHE changes its sign to positive. This behavior
 112 suggests that the reaction kinetics play a large role in the overall properties of the film. The
 113 applied voltage controls redox activity [27], thereby the generated hydrogen, which
 114 subsequently changes the film properties. Similar observations were reported in ref. [25],
 115 where the reaction kinetics were shown to be important in driving the film properties.

116



117

118 **Figure 4:** Hall resistance of PdCoO_2 films electrolytically processed for different duration at
 119 (a) -1.8 V, (b) -2.3 V, and (c) -3.5 V, measured at room temperature and 7 K.

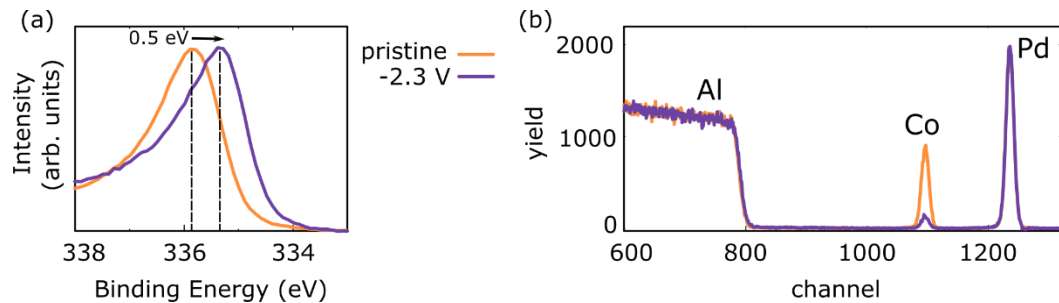
120 In contrast to room temperature, Hall effect at 7 K, as shown in Figure 4, exhibits well-
 121 defined hysteresis loops with large coercive fields, suggesting the presence of stable
 122 ferromagnetic domains with PMA. Nonetheless, the magnitude of the coercive field gradually
 123 decreases as the voltage increases, with the sign switched at -3.5 V. A bowknot shape is
 124 observed after 60 min electrolysis at -3.5 V, which is likely due to the presence of multiple
 125 transport channels with different AHE signs. The AHE results are reproducible across
 126 multiple samples.

127 The emergence of AHE suggests that the main outcome of the electrolytic process is
 128 reduction of the PdCoO_2 films into a ferromagnetic Pd-Co alloy, which subsequently exhibits
 129 sign-tunable AHE with the applied voltage. The XPS data in Figure 5(a) confirm that the
 130 films are reduced after the process. It is notable that the electrolytic process, which is distinct
 131 from the hydrogen annealing [25], can induce similar modification of the PdCoO_2 films.
 132 There are some differences as well: most significantly, hysteresis is lacking at room
 133 temperature in these samples unlike the hydrogen-annealed samples. This suggests that
 134 despite some similarities, the electrolytic process, driven by an electro-chemical force, results
 135 in different structures (and compositions) of Pd-Co alloys than the hydrogen annealing does
 136 for the PdCoO_2 films. Notably, a recent electrolytic study of PdCoO_2 bulk crystals

137 demonstrated that Co and O can leach into an acidic electrolyte leaving a Pd-rich capping
 138 layer [18]. In a similar manner, as shown in Figure 5(b), RBS comparing a pristine film and a
 139 film treated at -2.3 V for 60 mins shows significant loss of Co from the electrolytically
 140 treated film. This is in contrast with the hydrogen-annealed PdCoO₂ films, where Pd and Co
 141 contents remain intact through the process [25]. It is notable that even with the significant
 142 loss of Co, strong AHE signals are observed in the electrolytically-processed films.
 143 Considering that Pd is known to be on the verge of becoming ferromagnetic, even tiny
 144 amounts of Co can allow Pd to become ferromagnetic [28]. Moreover, Pd layer could also
 145 absorb hydrogen and form magnetic PdH_x [29]. These studies suggest that ferromagnetism,
 146 thus AHE, can emerge via multiple routes during electrolysis in PdCoO₂ films.

147

148



149 Figure 5: (a) XPS shows that Pd 3d_{5/2} spectrum shifts by about 0.5 eV to lower binding
 150 energies with an applied voltage of -2.3V, showing the reduced nature of the film treated at -
 151 2.3 V for 60 min. (b) RBS for the same film, showing significant loss of Co content after the
 152 electrolysis.

153

154

4. Conclusions

155 In conclusion, this work provides a way to change the nonmagnetic PdCoO₂ film into a
 156 reduced ferromagnetic material exhibiting perpendicular magnetic anisotropy. Above a
 157 threshold voltage of -1.2 V, the well-known water splitting potential, hydrogen is generated
 158 on the cathode and the film subsequently becomes ferromagnetic, and the anomalous Hall

159 effect can be tuned by the voltage applied during electrolysis. This study shows that
160 electrolysis could provide another route to manipulating magneto-electronic properties of
161 PdCoO₂ films for spintronic applications.

162

163 **Acknowledgement**

164 This work is supported by National Science Foundation, Grant No. DMR2004125 and Army
165 Research Office (ARO), Grant No. W911NF-20-1-0108. Y.L. acknowledges the state
166 scholarship provided by the China Scholarship Council.

167

168 **References**

169 [1] A.P. Mackenzie, The properties of ultrapure delafossite metals, *Reports Prog. Phys.* 80
170 (2017) 032501. <https://doi.org/10.1088/1361-6633/aa50e5>.

171 [2] R.D. Shannon, D.B. Rogers, C.T. Prewitt, Chemistry of noble metal oxides. I.
172 Syntheses and properties of ABO_2 delafossite compounds, *Inorg. Chem.* 10 (1971)
173 713–718. <https://doi.org/10.1021/ic50098a011>.

174 [3] C.T. Prewitt, R.D. Shannon, D.B. Rogers, Chemistry of Noble Metal Oxides. II.
175 Crystal Structures of PtCoO_2 , PdCoO_2 , CuFeO_2 , and AgFeO_2 , *Inorg. Chem.* 10 (1971)
176 719–723. <https://doi.org/10.1021/ic50098a012>.

177 [4] M. Tanaka, M. Hasegawa, H. Takei, Growth and Anisotropic Physical Properties of
178 PdCoO_2 Single Crystals, *J. Phys. Soc. Japan.* 65 (1996) 3973–3977.
179 <https://doi.org/10.1143/JPSJ.65.3973>.

180 [5] M. Tanaka, M. Hasegawa, H. Takei, Crystal growth of PdCoO_2 , PtCoO_2 and their
181 solid-solution with delafossite structure, *J. Cryst. Growth.* 173 (1997) 440–445.
182 [https://doi.org/10.1016/S0022-0248\(96\)00847-0](https://doi.org/10.1016/S0022-0248(96)00847-0).

183 [6] H. Takatsu, S. Yonezawa, S. Mouri, S. Nakatsuji, K. Tanaka, Y. Maeno, Roles of
184 high-frequency optical phonons in the physical properties of the conductive delafossite
185 PdCoO_2 , *J. Phys. Soc. Japan.* 76 (2007) 104701.
186 <https://doi.org/10.1143/JPSJ.76.104701>.

187 [7] M. Hasegawa, I. Inagawa, M. Tanaka, I. Shirotani, H. Takei, Thermoelectric power of
188 delafossite-type metallic oxide PdCoO_2 , *Solid State Commun.* 121 (2002) 203–205.
189 [https://doi.org/10.1016/S0038-1098\(01\)00484-7](https://doi.org/10.1016/S0038-1098(01)00484-7).

190 [8] K.P. Ong, D.J. Singh, P. Wu, Unusual transport and strongly anisotropic thermopower
191 in PtCoO_2 and PdCoO_2 , *Phys. Rev. Lett.* 104 (2010) 176601.
192 <https://doi.org/10.1103/PhysRevLett.104.176601>.

193 [9] M.E. Gruner, U. Eckern, R. Pentcheva, Impact of strain-induced electronic topological
194 transition on the thermoelectric properties of PtCoO_2 and PdCoO_2 , Phys. Rev. B. 92
195 (2015) 235140. <https://doi.org/10.1103/PhysRevB.92.235140>.

196 [10] K. Kim, H.C. Choi, B.I. Min, Fermi surface and surface electronic structure of
197 delafossite PdCoO_2 , Phys. Rev. B. 80 (2009) 035116.
198 <https://doi.org/10.1103/PhysRevB.80.035116>.

199 [11] V. Eyert, R. Fresard, A. Maignan, On the metallic conductivity of the delafossites
200 PdCoO_2 and PtCoO_2 , Chem. Mater. 20 (2008) 2370–2373.
201 <https://doi.org/10.1021/cm703404e>.

202 [12] K.P. Ong, J. Zhang, J.S. Tse, P. Wu, Origin of anisotropy and metallic behavior in
203 delafossite PdCoO_2 , Phys. Rev. B. 81 (2010) 115120.
204 <https://doi.org/10.1103/PhysRevB.81.115120>.

205 [13] R. Daou, R. Frésard, S. Hébert, A. Maignan, Large anisotropic thermal conductivity of
206 the intrinsically two-dimensional metallic oxide PdCoO_2 , Phys. Rev. B. 91 (2015)
207 041113(R). <https://doi.org/10.1103/PhysRevB.91.041113>.

208 [14] H.J. Noh, J. Jeong, J. Jeong, E.-J. Cho, S.B. Kim, K. Kim, B.I. Min, H.-D. Kim,
209 Anisotropic electric conductivity of delafossite PdCoO_2 studied by angle-resolved
210 photoemission spectroscopy, Phys. Rev. Lett. 102 (2009) 256404.
211 <https://doi.org/10.1103/PhysRevLett.102.256404>.

212 [15] M. Hasegawa, M. Tanaka, T. Yagi, H. Takei, A. Inoue, Compression behavior of the
213 delafossite-type metallic oxide PdCoO_2 below 10 GPa, Solid State Commun. 128
214 (2003) 303–307. <https://doi.org/10.1016/j.ssc.2003.08.037>.

215 [16] C.W. Hicks, A.S. Gibbs, A.P. Mackenzie, H. Takatsu, Y. Maeno, E.A. Yelland,
216 Quantum oscillations and high carrier mobility in the delafossite PdCoO_2 , Phys. Rev.
217 Lett. 109 (2012) 116401. <https://doi.org/10.1103/PhysRevLett.109.116401>.

218 [17] P.J.W. Moll, P. Kushwaha, N. Nandi, B. Schmidt, A.P. Mackenzie, Evidence for
219 hydrodynamic electron flow in PdCoO₂, *Science*. 351 (2016) 1061.
220 <https://doi.org/10.1126/science.aac8385>.

221 [18] F. Podjaski, D. Weber, S. Zhang, L. Diehl, R. Eger, V. Duppel, E. Alarcón-Lladó, G.
222 Richter, F. Haase, A. Fontcuberta i Morral, C. Scheu, B. V. Lotsch, Rational strain
223 engineering in delafossite oxides for highly efficient hydrogen evolution catalysis in
224 acidic media, *Nat. Catal.* 3 (2020) 55–63. <https://doi.org/10.1038/s41929-019-0400-x>.

225 [19] G. Li, S. Khim, C.S. Chang, C. Fu, N. Nandi, F. Li, Q. Yang, G.R. Blake, S. Parkin, G.
226 Auffermann, Y. Sun, D.A. Muller, A.P. Mackenzie, C. Felser, In Situ Modification of
227 a Delafossite-Type PdCoO₂ Bulk Single Crystal for Reversible Hydrogen Sorption and
228 Fast Hydrogen Evolution, *ACS Energy Lett.* 4 (2019) 2185–2191.
229 <https://doi.org/10.1021/acsenergylett.9b01527>.

230 [20] K. Toyoda, R. Hinogami, N. Miyata, M. Aizawa, Calculated descriptors of catalytic
231 activity for water electrolysis anode: Application to delafossite oxides, *J. Phys. Chem.*
232 C. 119 (2015) 6495–6501. <https://doi.org/10.1021/jp5092398>.

233 [21] R. Hinogami, K. Toyoda, M. Aizawa, T. Kawasaki, H. Gyoten, Copper Delafossite
234 Anode for Water Electrolysis, *ECS Trans.* 58 (2013) 27–31.
235 <https://doi.org/10.1149/05802.0027ecst>.

236 [22] K. Toyoda, R. Hinogami, N. Miyata, M. Aizawa, Catalyst Design of Delafossite
237 Oxides for Water Electrolysis Anode Using Theoretical Calculations, *ECS Trans.* 66
238 (2015) 1–4. <https://doi.org/10.1149/06633.0001ecst>.

239 [23] F. Mazzola, V. Sunko, S. Khim, H. Rosner, P. Kushwaha, O.J. Clark, L. Bawden, I.
240 Marković, T.K. Kim, M. Hoesch, A.P. Mackenzie, P.D.C. King, Itinerant
241 ferromagnetism of the Pd-terminated polar surface of PdCoO₂, *Proc. Natl. Acad. Sci.*
242 115 (2017) 12956. <https://doi.org/10.1073/pnas.1811873115>.

243 [24] T. Harada, K. Sugawara, K. Fujiwara, M. Kitamura, S. Ito, T. Nojima, K. Horiba, H.
244 Kumigashira, T. Takahashi, T. Sato, A. Tsukazaki, Anomalous Hall effect at the
245 spontaneously electron-doped polar surface of PdCoO_2 ultrathin films, *Phys. Rev. Res.*
246 2 (2020) 013282. <https://doi.org/10.1103/physrevresearch.2.013282>.

247 [25] G. Rimal, C. Schmidt, H. Hijazi, L.C. Feldman, Y. Liu, E. Skoropata, J. Lapano, M.
248 Brahlek, D. Mukherjee, R.R. Unocic, M.F. Chisholm, Y. Sun, H. Yu, S. Ramanathan,
249 C.-J. Sun, H. Zhou, S. Oh, Effective reduction of PdCoO_2 thin films via hydrogenation
250 and sign tunable anomalous Hall effect, *Phys. Rev. Mater.* 5 (2021) L052001.
251 <https://doi.org/10.1103/physrevmaterials.5.l052001>.

252 [26] M. Brahlek, G. Rimal, J.M. Ok, D. Mukherjee, A.R. Mazza, Q. Lu, H.N. Lee, T.Z.
253 Ward, R.R. Unocic, G. Eres, S. Oh, Growth of metallic delafossites by molecular beam
254 epitaxy, *Phys. Rev. Mater.* 3 (2019) 093401.
255 <https://doi.org/10.1103/PhysRevMaterials.3.093401>.

256 [27] G. Inzelt, Crossing the bridge between thermodynamics and electrochemistry. From
257 the potential of the cell reaction to the electrode potential, *ChemTexts.* 1 (2015) 2.
258 <https://doi.org/10.1007/s40828-014-0002-9>.

259 [28] R.M. Bozorth, P.A. Wolff, D.D. Davis, V.B. Compton, J.H. Wernick, Ferromagnetism
260 in dilute solutions of cobalt in palladium, *Phys. Rev.* 122 (1961) 1157–1160.
261 <https://doi.org/10.1103/PhysRev.122.1157>.

262 [29] X. Cui, X.X. Liang, J.T. Wang, G.Z. Zhao, Ab initio studies on the mechanic and
263 magnetic properties of PdH_x , *Chinese Phys. B.* 20 (2011) 026201.
264 <https://doi.org/10.1088/1674-1056/20/2/026201>.

265

266 List of Figures

267 **Figure 1:** Experiment setup. (a) Schematic diagram of the setup; (b) Underwater part of the
268 film. Also shown is the formation of hydrogen bubbles on the film surface when a voltage of
269 -5.0 V is applied.

270

271 **Figure 2:** Average two-point resistance ($R_{2\text{prb}}$) measured after a sample is kept in the
272 electrolyte (a) at the specified voltage for 5 minutes and (b) for the specified time at -1.0V, -
273 1.8 V, -2.3 V and -3.5 V. Four separate samples are used for (b). The negative voltages imply
274 that the PdCoO_2 film is used as a cathode.

275

276 **Figure 3:** Hall effect data ($R_{\text{Hall}} \equiv R_{xy}$) of PdCoO_2 thin films measured at room temperature
277 after electrolytic processing at (a) -1.0 V, (b) -1.8 V, (c) -2.3 V and (d) -3.5 V.

278

279 **Figure 4:** Hall resistance of PdCoO_2 films electrolytically processed for different duration at
280 (a) -1.8 V, (b) -2.3 V, and (c) -3.5 V, measured at room temperature and 7 K.

281

Figure 5: (a) XPS shows that $\text{Pd } 3\text{d}_{5/2}$ spectrum shifts by about 0.5 eV to lower binding
energies with an applied voltage of -2.3V, showing the reduced nature of the film treated at -
2.3 V for 60 min. (b) RBS for the same film, showing significant loss of Co content after the
electrolysis.